Characteristic Mode Analysis of Multi-Octave Asymmetric Dipoles

Characteristic Mode Analysis of Multi-Octave Asymmetric Dipoles

A. Tibaldi*†, G. Virone†, P. Bolli‡, F. Paonessa† G. Addamo† O. A. Peverini† M. Lumia† L. Ciorba*†
*Dipartimento di Elettronica e Telecomunicazioni, Politecnico di Torino, Torino, Italy, alberto.tibaldi@polito.it
†Istituto di Elettronica e di Ingegneria dell'Informazione e delle Telecomunicazioni (IEIIT), CNR, Torino, Italy
‡Osservatorio Astrofisico di Arcetri, Istituto Nazionale di Astrofisica (INAF), Firenze, Italy

***Abstract*—This paper discusses the impedance and front-to-back ratio performance of asymmetric dipoles. These parameters are very important when the antennas are placed over a conductive ground plane and should operate over multi-octave frequency bands. The operation of these antennas is usually described relying on analogies with more classical structures such as symmetric dipoles and tapered slot antennas. To provide a solid theoretical background to this intuition, this work presents the application of characteristic mode analysis to multi-octave dipole antennas. Firstly, a brief review of the main characteristic mode content is presented. Then, characteristic mode analysis is applied to three antenna concepts to emphasize how their geometry impacts on the relevant figures of merit. This allows to draw some conclusions on the achievable performance by different designs.**

***Index Terms*—antenna design, asymmetric dipoles, characteristic mode analysis.**

I. Introduction

Several applications require the design of compact broadband antennas that can be placed over a ground plane. For instance, the guidelines of the Square Kilometer Array (SKA) [1] require a 7:1 bandwidth with minimum ripple on the overall antenna directivity, the presence of a ground plane is required in order to decouple the array elements from the soil ground. To this end, omnidirectional dipoles over a ground plane cannot be adopted owing the cancellation that occurs when the distance between the antenna and the ground approaches $\lambda/2$. On the contrary, a high front-to-back ratio is required to make the antenna insensitive to the ground across the whole frequency band. Driven by the manufacturing simplicity and cost-effectiveness of asymmetrical dipole antennas (see Fig. 1), this work investigates their front-to-back ratio performance.

In the literature, the operation of multi-octave asymmetrical dipoles is commonly described by invoking analogies with more classical configurations. At low frequencies the antenna asymmetry is not very significant, it basically operates as a small dipole with a quasi-omnidirectional pattern (see Fig. 2). On the contrary, at high-frequencies the currents are more concentrated on the inner edges (tapered-slot, Vivaldi antenna [2], [3]) and a higher directivity behavior is achieved. The full band operation is supposed to result from the combination of these two mechanisms [4], [5]. However, this intuition lacks a solid theoretical background capable of interpreting rigorously the antenna operation and then give some room for design optimization.

In this view, an interesting antenna simulation framework is provided by characteristic mode analysis (CMA). Presented in the early '70s in the pioneering papers of Garbacz and Harrington [6], [7], CMA is experiencing a renewed interest, being an enabling methodology to approach electromagnetic modeling from a physical- rather than merely numerical-oriented standpoint [8], [9]. Being implemented in commercial electromagnetic integral equation solvers (*e.g.* Altair FEKO or CST Microwave Studio), this technique has been recently employed in many applications, such as bandwidth enhancement for MIMO antenna systems [10], [11], design of pattern-reconfigurable null-scanning radiators [12], or placement optimization in aircrafts [13].

This communication is aimed at presenting the application of CMA to multi-octave dipoles. Firstly, the main CMA concepts and notations are reviewed in Section II. Then, in Section III the technique is applied to the analysis of the three antenna concepts sketched in Fig. 1. A discussion of the simulation results allows to establish a solid interpretation of the antenna operation in terms of interference between several characteristic modes, leading to the design considerations and to the conclusions reported in Section IV. All the simulations presented in this paper have been performed with the method of moments (MoM) simulator FEKO from Altair HyperWorks v2017.1.

II. Review of Characteristic Mode Analysis

The characteristic mode analysis (CMA) is based on a post-processing of the impedance matrix $\mathcal{Z}$ obtained from the application of the method of moments to the electric field integral equation for perfect electric conductor scatterers. By defining the resistance and reactance operators $\mathcal{R}$ and $\mathcal{X}$ from $\mathcal{Z}$, the following generalized eigenproblem is obtained:

$$\mathcal{X}\mathbf{J}_n = \lambda_n \mathcal{R}\mathbf{J}_n. \tag{1}$$

Being the operators in (1) real and symmetric, both the eigencurrents $\{\mathbf{J}_n\}$ and the corresponding eigenvalues $\{\lambda_n\}$ representing the "characteristic modes" of the antenna under simulation are real. By exploiting the orthogonality relationships of the eigencurrents reported in [6, eq. (14)], it is possible

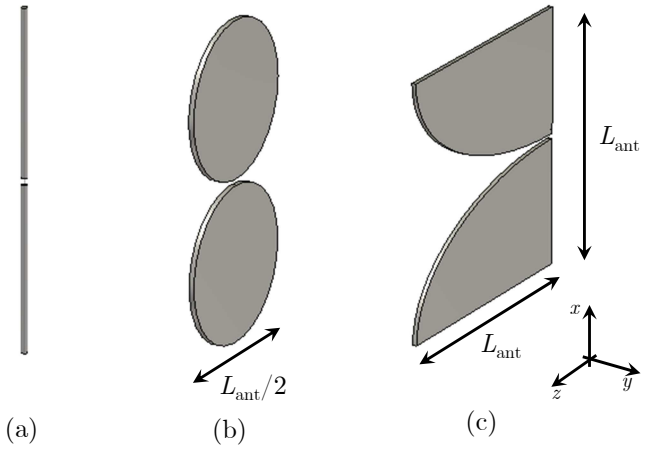

Fig. 1. Sketches of three antenna concepts: a cylindrical dipole (a), a circular dipole (b), an asymmetrical dipole (Vivaldi) (c).

to compute the power flux radiated by the overlap of two eigencurrents,

$$P_s = \langle \mathbf{J}_m^*, \mathcal{Z}\,\mathbf{J}_n \rangle = (1 + j\lambda_n)\delta_{mn}, \tag{2}$$

which states that the eigenvalue λ_n can be interpreted as a measure of the reactive contribution to the power radiated by the n-th eigencurrent.

In order to apply CMA to real antenna problems, it is necessary to expand the current density $\mathbf{J}$ describing the scattering of the source electric field $\mathbf{E}^{(inc)}$ by the antenna surface as a linear combination of the eigencurrents from (1), leading to

$$\mathbf{J} = \sum_n \alpha_n \mathbf{J}_n, \tag{3}$$

where the n-th modal weighting coefficient of $\mathbf{J}$ in the eigencurrent basis $\{\mathbf{J}_n\}$ is

$$\alpha_n = \frac{1}{1 + j\lambda_n} V_n^{(inc)}. \tag{4}$$

Two contributions can be identified. The modal excitation coefficient $V_n^{(inc)}$ measures the power coupled by $\mathbf{E}^{(inc)}$ to the n-th eigencurrent, and it is defined as the projection $V_n^{(inc)} = \langle \mathbf{J}_n, \mathbf{E}^{(inc)} \rangle$. The remaining term $(1 + j\lambda_n)^{-1}$, which depends exclusively on the geometry of the scatterer (and then is independent of the source field), quantifies the capability to couple power to the n-th mode. From its magnitude, which is commonly referred to as modal significance, it is apparent that the maximum coupling occurs at the resonance condition $\lambda_n = 0$.

III. CMA ANALYSIS OF BROADBAND DIPOLE ANTENNAS

The first part of this section presents some considerations on the reflection coefficient of dipole antennas, with reference to the three antenna concepts sketched in Fig. 1. Figure 4 reports the reflection coefficients for these three antennas (top), and, below, the most significant modal weighting coefficients α_n are reported. Focusing on the cylindrical dipole having aspect ratio $L_{ant}/r = 120$, being r the dipole radius, the reflection dips occur for $L_{ant} \simeq 0.4\lambda$ and $L_{ant} \simeq 1.4\lambda$, which are related to the first and third resonances of a half-wavelength dipole. No contribution from the second resonance can be observed. Indeed, even if the corresponding modal significance $|1 + j\lambda_2|^{-1}$ from (4) is high, the corresponding excitation coefficient $V_2^{(inc)}$ is zero. This is a consequence of the presence of a zero of the eigencurrent in the antenna center, making it impossible to be excited by a centered feed. To summarize, since the reflection dips correspond exactly to the weighting coefficient peaks, it is possible to identify the dipole resonances with the first and third characteristic modes of the structure.

By extending this analysis to the other two antennas, it is possible to observe similar low-frequency trends: the reflection coefficient is quite high correspondingly to low modal weighting, until the first resonance is achieved. The different positions of the first peak (see Fig. 4, middle row) can be ascribed to the different transverse dimensions of the dipoles (the Vivaldi antenna has the largest surface area).

At high frequencies, a major difference between cylindrical and broadband dipoles can be immediately noticed. In the former, the weighting coefficient of the fundamental mode reduces in favor of the higher-order one. On the contrary, in the broadband antennas the fundamental mode is dominant across almost the entire frequency band, but several high-order modes contribute to the overall operation. Nevertheless, the minima of the reflection coefficients still correspond to the peaks of the modal weighting coefficients.

Figure 4 (bottom right) reports the front-to-back ratio (FBR) only for the Vivaldi antenna (as the other ones are identically equal to 0 dB). In the low-frequency region the FBR is approximately 0 dB. As a matter of fact, Fig. 2 shows an example of Vivaldi radiation pattern obtained for $L_{ant} = 0.2\lambda$. This plot strengthens the common interpretation of low-frequency behavior as "dipole-like". At higher frequencies, it can be observed that FBR reaches high levels (> 15 dB) in several subbands. However, 10 dB level are present elsewhere. This limits the operation frequency range in presence of ground plane.

In order to provide more details about the Vivaldi directivity behavior, Fig. 3 (left) shows the radiation pattern of the Vivaldi antenna at $L_{ant} = \lambda$ where, according to Fig. 4, the FBR is maximum. The corresponding eigenpattern magnitudes (a)-(c) are reported on the right. At first sight the eigenpatterns could seem unreasonable, since they appear perfectly symmetric even for such an asymmetric geometry. This symmetry is a consequence of the fact that eigencurrents $\mathbf{J}_n$ are real-valued functions and the radiated eigenpatterns are computed by their Fourier transforms. A real function in the starting domain is then transformed in a function with even magnitude and odd phase in the angular (dual) domain. This is shown in Fig. 5 (right), which reports the magnitudes and phases (top, center) of the three most significant eigenpatterns, exhibiting the aforementioned symmetries. The three-mode pattern re-

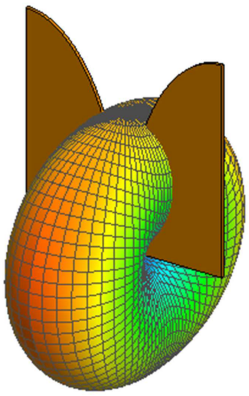

Fig. 2. Radiation pattern of the Vivaldi antenna sketched in Fig. 1(c) for $L_{ant} = 0.2\lambda$.

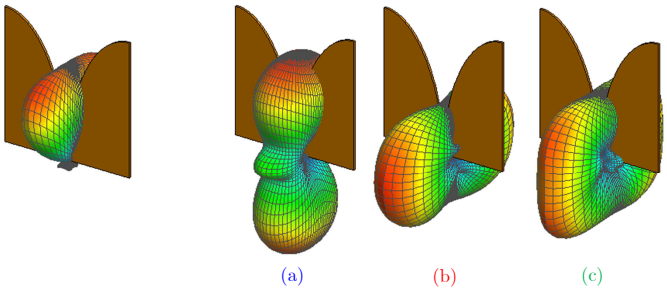

Fig. 3. Radiation patterns of the Vivaldi antenna sketched in Fig. 1(c) for $L_{ant} = \lambda$. Left: radiation pattern under excitation. Right: eigenpatterns for the three fundamental characteristic modes, where the colors of the labels (a)-(c) correspond to the modal weighting coefficients reported in Fig. IV (right).

construction (dashed red curve) exhibits the expected directive behavior. This is not the case of the two-mode representation (dashed brown curve), which is sensitively different from the reference MoM solution.

It could be seen that also the other FBR peaks result from this peculiar three-mode interference. As an example, Fig. 4 shows similar results for the first FBR peak at $L_{ant} = 0.45\lambda$.

IV. Design Considerations and Conclusions

The characteristic mode analysis allows to clarify several aspects of the working principle of broadband dipoles, which are now summarized in view of proposing some design considerations.

In the first place, the intuition of Vivaldi to behave as symmetrical dipoles at low frequencies has been better interpreted. This definitely states that high FBR cannot be achieved for electrically small antennas, where only one mode is significant (eigenpatterns have symmetrical magnitude).

At higher frequencies, it has been shown that the directive behavior results from the interference of several characteristic modes. In the antennas discussed in this work a unique feed is present. This generally excites more than one mode and hence the surface current results from the linear combination of the frequency-dependent eigencurrents by complex-valued coefficients (4). This is quite different from most CMA applications, which exploit the orthogonality of the eigencurrents to optimize the antenna feed to obtain peculiar designs [10], [11], [13].

The interference of characteristic modes produces a significant frequency variation of the FBR. As a matter of fact, their cancellation in the backlobe direction, only occurs at certain frequencies where a proper phase condition is satisfied. Therefore, for antennas supporting only a few modes, it is not possible to achieve a high and stable FBR across a broadband. This consideration is almost independent of the asymmetrical dipole geometry. This behavior has been also verified on asymmetrical dipoles with exponential and piecewise profiles.

References

[1] P. E. Dewdney, P. J. Hall, R. T. Schilizzi, and T. J. L. W. Lazio, "The square kilometre array," *Proc. IEEE*, vol. 97, no. 8, pp. 1482–-1496, Aug. 2009.

[2] D. H. Schaubert, "A class of E-plane scan blindnesses in single-polarized arrays of tapered-slot antennas with a ground plane," *IEEE Trans. Antennas Propag.,* vol. 44, no. 7, pp. 954–959, July 1996.

[3] D. H. Schaubert, S. Kasturi, A. O. Boryssenko, and W. M. Elsallal, "Vivaldi antenna arrays for wide bandwidth and electronic scanning," *2nd European Conference on Antennas and Propagation (EuCAP 2007)*, Nov. 2007, Edinburgh.

[4] A. Tibaldi, G. Virone, F. Perini, J. Monari, M. Z. Farooqui, M. Lumia, O. A. Peverini, G. Addamo, R. Tascone and R. Orta, "Design considerations for a low-frequency Vivaldi array element," *PIERS,* Stockholm, Aug. 2013.

[5] J. Monari, F. Perini, M. Schiaffino, G. Bianchi, A. Mattana, G. Naldi, G. Pupillo, G. Tartarini, S. Rusticelli, G. Virone, A. Tibaldi, R. Tascone, O. A. Peverini, G. Addamo, P. Debernardi, A. M. Lingua, M. Piras, A. Cina, P. Maschio, and H. Bendea, "Aperture array for low frequency: the Vivaldi solution," *ICEAA,* Torino, Sept. 2013.

[6] R. F. Harrington and J. R. Mautz, "Theory of characteristic modes for conducting bodies," *IEEE Trans. Antennas Propag.,* vol. AP-19, no. 5, Sept. 1971.

[7] R. J. Garbacz and R. H. Turpin, "A generalized expansion for radiated and scattered fields," *IEEE Trans. Antennas Propag.,* vol. AP-19, no. 5, May. 1971.

[8] G. Addamo, D. Bekers, A. G. Tijhuis, B. P. De Hon, R. Orta and R. Tascone, "An Eigencurrent Approach for the Analysis of Leaky Coaxial Cables," *1st European Conference on Antennas and Propagation (EuCAP 2006),* Nov. 2006.

[9] M. Cabedo-Fabrés, E. Antonino-Daviu, A. Valero-Nogueira, and M. Ferrando Bataller, "The theory of characteristic modes revisited: a contribution to the design of antennas for modern applications," *IEEE Antennas Propag. Mag.,* vol. 49, no. 5, pp. 52-68, Oct. 2007.

[10] R. Martens, J. Holopainen, E. Safin, J. Ilvonen, and D. Manteuffel, "Optimal dual-antenna design in a small terminal multiantenna system," *IEEE Antennas Wireless Propag. Lett.,* vol. 12, pp. 1700-1703, Dec. 2013.

[11] Z. Miers, H. Li, and B. K. Lau, "Design of bandwidth-enhanced and multiband MIMO antennas using characteristic modes," *IEEE Antennas Wireless Propag. Lett.,* vol. 12, pp. 1696-1699, Dec. 2013.

[12] F. A. Dicandia, S. Genovesi, and A. Monorchio, "Advantageous exploitation of characteristic modes analysis for the design of 3-D null-scanning antennas," *IEEE Trans. Antennas Propag.,* vol. 65, no. 8, pp. 3924-3934, Aug. 2017.

[13] M. H. Vogel, W. J. Strydom, U. Jakobus, and P. Futter, "Aircraft antenna placement using characteristic modes," *11th European Conference on Antennas and Propagation (EuCAP 2017)*, March 2017, Paris

[14] C. J. Lonsdale, R. J. Cappallo, *et al.*, "The Murchison widefield array: design overview," *Proc. IEEE,* vol. 97, no. 8, pp. 1497-1506, Aug. 2009.

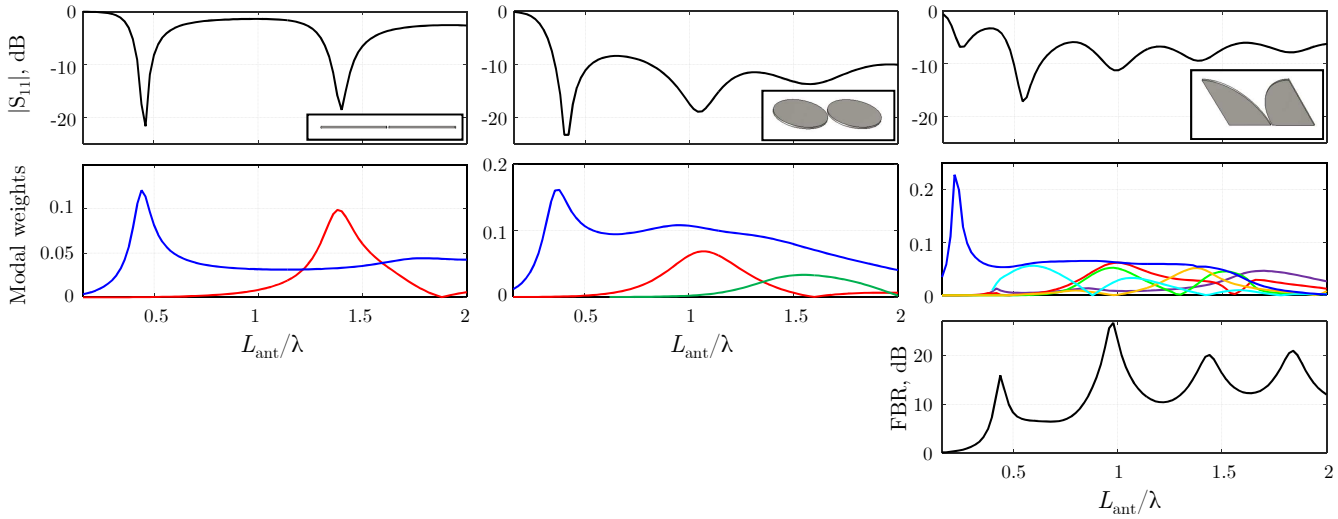

Fig. 4. The top plots report the antenna reflection coefficients for the cylindrical dipole (left, 75 Ω impedance), circular dipole (center, 50 Ω impedance) and Vivaldi antenna (right, 50 Ω impedance). Below are reported the absolute values of the corresponding modal weighting coefficients α_n related to the most significant characteristic modes. The front-to-back ratio (FBR) is reported only for the Vivaldi antenna.

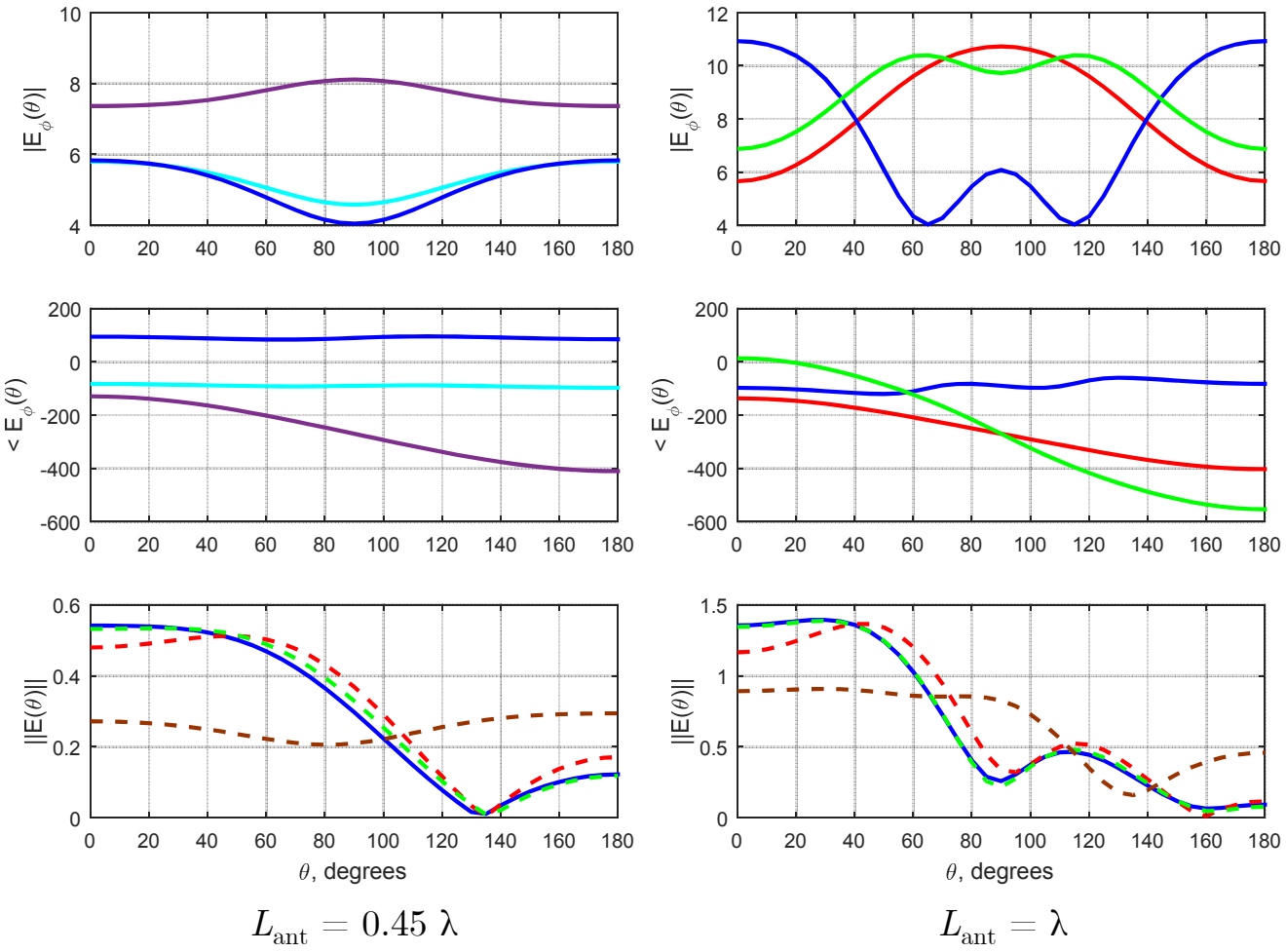

Fig. 5. The top and central plots show the magnitude and phase of the Vivaldi eigenpatterns. The colors are consistent to ones in Fig. IV (right). The bottom plot shows the radiation pattern obtained with the standard MoM solution (solid blue curve) and with the characteristic mode analysis rebuilt with all (dashed green curve), three (dashed red curve) and two (dashed brown curve) characteristic modes. Left and right figures are obtained with $L_{ant} = 0.45\lambda$ and $L_{ant} = \lambda$, respectively